SIAM J. SCI. COMPUT.
Vol. 41, No. 3, pp. B448–B465

A HIGH ORDER POSITIVITY PRESERVING DG METHOD FOR COAGULATION-FRAGMENTATION EQUATIONS*

HAILIANG LIU†, ROBIN GRÖPLER‡, AND GERALD WARNECKE‡

Abstract. We design, analyze, and numerically validate a novel discontinuous Galerkin (DG) method for solving the coagulation-fragmentation equations. The DG discretization is applied to the conservative form of the model, with flux terms evaluated by Gaussian quadrature with $Q = k + 1$ quadrature points for polynomials of degree k. The first moment (total mass) is naturally conserved by the scheme construction, and the positivity of the mass density is enforced by the use of a scaling limiter based on positive cell averages. The positivity of cell averages is shown to propagate by the time discretization, provided a proper time step restriction is imposed.

Key words. population balance equation, aggregation, breakage, conservation law, discontinuous Galerkin method, high order accuracy

AMS subject classifications. 65M60, 65M12, 65R20, 35L65, 82C22

DOI. 10.1137/17M1150360

1. Introduction.

Aggregation-breakage population balance equations (PBEs) are the models for the growth of particles by the combined effect of aggregation and breakage. These equations are a type of partial integro-differential equations which are also known as coagulation-fragmentation equations. These models describe the dynamics of particle growth and the time evolution of a system of particles under the combined effect of aggregation, or coagulation, and breakage, or fragmentation. Each particle is identified by its size, or volume, which is assumed to be a positive real number. From a physical point of view, the basic mechanisms taken into account are the coalescence of two particles to form a larger one and the breakage of particles into smaller ones. These models are of substantial interest in many areas of science and engineering [1, 23, 32, 34].

The equations we consider in this paper describe the time evolution of the particle size distribution (PSD) under the simultaneous effect of binary aggregation and multiple breakage. The objective of this work is to design a high order discontinuous Galerkin method for these equations, so that the numerical solution is highly accurate and remains nonnegative.

In 1917, Smoluchowski [39] proposed the discrete aggregation model in order to describe the coagulation of colloids moving according to a Brownian motion which is known as the Smoluchowski coagulation equation. In 1928, Müller [31] provided the continuous version of this equation as

$$\partial_t f(t,x) = \frac{1}{2}\int_0^x K(x-y,y)f(t,x-y)f(t,y)dy - \int_0^\infty K(x,y)f(t,x)f(t,y)dy,$$

*Submitted to the journal's Computational Methods in Science and Engineering section October 6, 2017; accepted for publication (in revised form) March 27, 2019; published electronically May 21, 2019.

http://www.siam.org/journals/sisc/41-3/M115036.html

Funding: The first author's research was partially supported by the National Science Foundation under grants DMS-1312636 and DMS-1107291. The second author's research was partially supported by the German Research Foundation DFG, GRK 1554.

†Department of Mathematics, Iowa State University, Ames, IA 50011 (hliu@iastate.edu).

‡Institute for Analysis and Numerics, Otto von Guericke University Magdeburg, 39106 Magdeburg, Germany (robin.groepler@online.de, warnecke@ovgu.de).

with $f(0,x) = f_0(x)$. Here the variables $x \geq 0$ and $t \geq 0$ denote the size of the particles and time, respectively. The number density of particles of size x at time t is denoted by $f(t,x)$. The coagulation kernel $K(x,y) \geq 0$ represents the rate at which the particles of size x coalesce with particles of size y and is assumed to be symmetric, i.e., $K(x,y) = K(y,x)$.

Later, analogous models for breakage or fragmentation were developed [29, 42, 43]. The continuous version of the coagulation and multiple fragmentation equations has been investigated; one of the models is of the form

$$\partial_t f(t,x) = \frac{1}{2}\int_0^x K(x-y,y)f(t,x-y)f(t,y)dy - \int_0^\infty K(x,y)f(t,x)f(t,y)dy + \int_x^\infty b(x,y)S(y)f(t,y)dy - S(x)f(t,x). \tag{1.1}$$

Here the breakage function $b(x,y)$ is the probability density function for the formation of particles of size x from the particles of size y. It is nonzero only for $x < y$. The selection function $S(x)$ describes the rate at which particles of size x are selected to break. The selection function S and breakage function b are defined in terms of the multiple-fragmentation kernel $\Gamma(x,y)$ as

$$S(x) = \int_0^x \frac{y}{x}\,\Gamma(x,y)dy, \quad b(x,y) = \Gamma(y,x)/S(y).$$

This equation is usually referred to as the generalized coagulation-fragmentation equation, as fragmenting particles can split into more than two pieces. Under some growth conditions, solutions are shown to exist in the space

$$X = \left\{ f \in L^1 : \int_0^\infty (1+x)f dx < \infty,\ f \geq 0 \text{ a.e.} \right\}$$

for nonnegative initial data $f_0 \in X$.

In aggregation-breakage processes, the total number of particles varies in time while the total mass of particles remains conserved. In terms of f, the total number of particles and the total mass of particles at time $t \geq 0$, respectively, are given by the moments

$$M_0(t) := \int_0^\infty f(t,x)dx, \quad M_1(t) := \int_0^\infty x f(t,x)dx.$$

It is easy to show that the total number of particles $M_0(t)$ decreases by aggregation and increases by breakage processes while the total mass $M_1(t)$ does not vary during these events. The total mass conservation

$$M_1(t) = M_1(0)$$

holds. However, for some special cases of K when it is sufficiently large compared to the selection function S, a phenomenon called gelation which has to do with a phase transition occurs. In this case, the total mass of particles is not conserved; see Escobedo et al. [10] and further citations for details.

Writing the aggregation and breakage terms in divergence form enables us to get a precise amount of mass dissipation or conservation. The mass balance formulation of (1.1) in terms of the mass density $n(t,x) = xf(t,x)$ takes the form

$$\partial_t n(t,x) + \partial_x F(t,x) = 0, \tag{1.2}$$

subject to the initial and boundary conditions $n(0,x) = n_0(x) \geq 0$ a.e. and $n(t,0) = 0$.

The nonlocal flux $F(t,x) = F_a(t,x) + F_b(t,x)$ is a weighted integral of functions in terms of $n(t,x)$. The aggregation flux is

$$F_a(t,x) := \int_0^x \int_{x-u}^{\infty} A(u,v)n(t,u)n(t,v)dvdu, \quad A(u,v) = K(u,v)/v,$$

and the breakage flux is

$$F_b(t,x) = -\int_x^{\infty} \int_0^x B(u,v)n(t,v)dudv, \quad B(u,v) = ub(u,v)S(v)/v,$$

where $A(u,v)$ and $B(u,v)$ are the weight functions. It should be noted that both forms of aggregation-breakage PBEs (1.1) and (1.2) are interchangeable by using the Leibniz integration rule. It should also be mentioned that (1.2) reduces to the case of a pure aggregation or pure breakage process when F_b or F_a is zero, respectively.

Mathematical results on existence and uniqueness of solutions of (1.1) and further citations can be found in McLaughlin, Lamb, and McBride [28] and Lamb [21] for rather general aggregation kernels, breakage, and selection functions. However, the equation can only be solved analytically for a limited number of simplified problems; see Ziff [42] and Dubovskii, Galkin, and Stewart [7] and the references therein. This leads to the necessity of using numerical methods for solving general equations. Several such numerical methods have been introduced. Stochastic methods (Monte Carlo) have been developed; see Lee and Matsoukas [22] for solving equations of aggregation with binary breakage. Finite element techniques can be found in Mahoney and Ramkrishna [26] and the references therein for the equations of simultaneous aggregation, growth, and nucleation. Some other numerical techniques are available in the literature, such as the method of successive approximations by Ramkrishna [34], the method of moments [25, 27], finite volume methods [30, 17], and sectional methods, such as the fixed pivot and the cell average technique [15, 19, 40], to solve such PBEs. There also exist spline methods [8] and a discontinuous Galerkin (DG) method [36] for the aggregation process. All these methods are applied to the standard form of the aggregation-breakage equation and have to deal with the problem of mass conservation.

An alternative numerical approach is based on the mass balance formulation. An application of a finite volume scheme (FVS) was introduced by Filbet and Laurençot [11] for solving the aggregation problem. Further, Bourgade and Filbet [2] have extended their scheme to solve the case of binary aggregation and binary breakage PBEs. For a special case of a uniform mesh, they have shown error estimates of first order. Kumar et al. [16] treated the case of aggregation and multiple breakage. The scheme has also been extended to two-dimensional aggregation problems by Qamar and Warnecke [33]. Finally, it has been observed that the FVS is a good alternative to the methods mentioned above for solving the PBEs due to its automatic mass conservation property. An analysis of the finite volume method to solve the aggregation with multiple breakage PBEs on general meshes is given in [18].

In this paper, we exploit the conservation formulation coupled with DG spatial discretization to solve (1.1). The DG method is a finite element method using a completely discontinuous piecewise polynomial space for the numerical solution and the test functions. Hence the method presented in this work may be seen as a natural extension of the above FVSs. In general, a DG method can easily handle unstructured meshes and local spaces of different types, and thus it is flexible for *hp*-adaptivity.

More general information about DG methods for elliptic, parabolic, and hyperbolic PDEs can be found in the recent books and lecture notes; see, e.g., [13, 35, 38].

The application of DG methods to first order hyperbolic problems has been quite successful; see Cockburn and Shu [6] for solving convection-dominated problems. The DG method [6] for local hyperbolic conservation law equations, $F = F(n(t,x))$, has a key advantage of local solvability, with communication between neighboring cells realized by the choice of a numerical flux $F_h = F_h(n^-, n^+)$. The application here is for an integro-differential equation (1.2) which poses additional difficulties. A crucial difference is that the numerical flux reduces to $F_h = F_h(t, x_{j+1/2})$ at interface $x_{j+1/2}$, yet this interface flux needs to be carefully evaluated in terms of numerical polynomials in all involved cells. We shall do so by adapting Gaussian quadratures to the present situation.

Important properties of such schemes including conservation of the first moment (total mass) and positivity of the mass density are proven for the scheme. The first is preserved by the construction, and the second by the use of a scaling limiter presented by Zhang and Shu [41] for general scalar conservation laws. The main idea in [41] is to find a sufficient condition to preserve the positivity of the cell averages by repeated convex combinations, so that DG methods with some scaling limiter satisfy the maximum principle for scalar conservation laws. Unfortunately, the way to find sufficient conditions in [41] cannot be applied to nonlocal PDEs such as (1.2) in a straightforward manner. We carefully select quadratures to both maintain the high order accuracy and preserve the positivity of the cell averages. This is achieved by further overcoming some new difficulties in identifying the CFL condition. To our best knowledge, the method is novel, and the techniques introduced here may be useful for other nonlocal PDEs. In addition, the extensive numerical results clearly demonstrate that the method performs very well.

From the known results for local conservation laws, we know that a proper time discretization with matching accuracy is often needed to make the fully discrete scheme stable. For scalar local conservation laws, it was shown in [3] that the DG method with P^1 elements in space and the Euler forward method in time is stable only if the CFL number is of order $\sqrt{\Delta x}$, which is a very restrictive condition. A slope limiter was then used as a way to improve the scheme stability. An obvious drawback in such a treatment is that the limiter has to balance the spurious oscillations in smooth regions caused by the use of a lower order time discretization. These difficulties were further overcome by the Runge–Kutta DG (RKDG) method of Cockburn and Shu [4, 5]. Such stable methods essentially involve three ingredients: (1) a high order DG method for space discretization, (ii) an RK method with matching accuracy for time discretization, and (iii) a limiter to dampen solution oscillations. In subsection 4.2, by our DG scheme using P^3 polynomials for space discretization and RK4 for time discretization, we have a comparison to show the blow-up of the numerical solutions if the limiter is not imposed. This numerical experiment has clearly demonstrated why the positivity-preserving technique is important.

This paper is organized as follows. First, we derive the DG scheme to solve aggregation-breakage PBEs in section 2. Then in section 3 details of the implementation are given. Later on, the scheme is numerically tested for several problems in section 4. Further, section 5 summarizes some conclusions.

2. Method description. In this section, a DG method for solving aggregation-breakage PBEs is discussed, following [11] for aggregation and [16] for multiple breakage.

In the PBE (1.2), the volume variable x ranges from 0 to ∞. In order to apply a numerical scheme for the solution of the equation, a first step is to truncate the problem and fix a finite computational domain $\Omega := [0, L]$ for a $0 < L < \infty$.

2.1. DG formulation. We develop a DG method for (1.2) subject to initial data $n_0(x)$. Let us partition the interval $\Omega = [0, L]$ into $0 = x_{1/2}, x_{3/2}, \ldots, x_{N+1/2} = L$ to get N subintervals and denote each cell by $I_j = (x_{j-1/2}, x_{j+1/2}]$, $j = 1, \ldots, N$. Each cell has the length $h_j = x_{j+1/2} - x_{j-1/2}$, and we set $h = \max_j h_j$ to be the mesh size. The representative of each cell, usually the center of each cell, $x_j = \frac{1}{2}\left(x_{j-1/2} + x_{j+1/2}\right)$, is called the pivot or grid point. The piecewise polynomial space V_h^k is defined as the space of polynomials of degree up to k in each cell I_j, that is,

$$V_h^k = \{v : v|_{I_j} \in P^k(I_j),\ j = 1, \ldots, N\}. \tag{2.1}$$

Note that functions in V_h^k are allowed to have discontinuities across cell interfaces.

The DG scheme is defined as follows: find $n_h \in V_h^k$ such that

$$\int_{I_j} \partial_t n_h \phi \, dx - \int_{I_j} F_h \partial_x \phi \, dx + F_h \phi \,\big|_{\partial I_j} = 0 \tag{2.2}$$

for all test functions ϕ in the finite element space V_h^k. Here we use the notation $v|_{\partial I_j} = v(x_{j+1/2}^-) - v(x_{j-1/2}^+)$, and $F_{j+1/2} = F_h(t, x_{j+1/2})$ is an appropriate approximation of the continuous flux function $F(t, x_{j+1/2})$. In case of a breakage process, the numerical flux may be approximated from the mass flux F_b, and similarly for the aggregation problem with flux F_a. In general, we have $F_{j+1/2} = F_{a,j+1/2} + F_{b,j+1/2}$. The initial condition $n_h(0, x) \in V_h^k$ is generated by the piecewise L^2 projection of $n_0(x)$, that is,

$$\int_0^L \left(n_h(0, x) - n_0(x)\right) \phi(x) dx = 0 \quad \text{for any } \phi \in V_h^k.$$

The semidiscrete DG scheme (2.2) is complete.

2.2. Flux evaluation. For the numerical integration of the fluxes, we use Gaussian quadrature of order Q with the Gauss evaluation points $s_\alpha \in (-1, 1)$ and the weights $\omega_\alpha > 0$:

$$\int_a^b g(u)du = \tfrac{b-a}{2} \int_{-1}^1 g\left(\tfrac{b+a}{2} + \tfrac{b-a}{2} s\right) ds = \tfrac{b-a}{2} \sum_{\alpha=1}^{Q} \omega_\alpha \, g\left(\tfrac{b+a}{2} + \tfrac{b-a}{2} s_\alpha\right) + R_Q, \tag{2.3}$$

where $R_Q = \mathcal{O}\left((b-a)^{2Q}\right)$ is the approximation residual, which is zero when g is a polynomial of degree at most $2Q - 1$. We will later use $Q = k + 1$; see Remark 2.1.

First, consider the boundary term in the DG scheme (2.2). Denote the quadrature points in I_j as $\hat{x}_j^\alpha = x_j + \frac{h_j}{2} s_\alpha$ for $\alpha = 1, \ldots, Q$. Then the aggregation flux

$$F_a(t, x_{j+1/2}) = \int_0^{x_{j+1/2}} \int_{x_{j+1/2}-u}^{x_{N+1/2}} A(u, v) n_h(t, u) n_h(t, v) dv du = \sum_{l=1}^{j} \int_{I_l} n_h(t, u) \Gamma_j(u) du$$

with the partial flux

$$\Gamma_j(u) = \int_{x_{j+1/2}-u}^{x_{N+1/2}} A(u, v) n_h(t, v) dv$$

is approximated by the numerical flux

$$F_{a,j+1/2} = \sum_{l=1}^{j} \frac{h_l}{2} \sum_{\alpha=1}^{Q} \omega_\alpha n_h(t, \hat{x}_l^\alpha) \Gamma_{j,l}^\alpha, \tag{2.4}$$

where $\Gamma_{j,l}^\alpha$ is an approximation to the partial flux $\Gamma_j(\hat{x}_l^\alpha)$ applying Gaussian quadrature, which we explain below. Let the index J be chosen such that $x_{j+1/2} - \hat{x}_l^\alpha \in I_J$, that is, $x_{J-1/2} < x_{j+1/2} - \hat{x}_l^\alpha \le x_{J+1/2}$; then

$$\Gamma_j(\hat{x}_l^\alpha) = \int_{x_{j+1/2}-\hat{x}_l^\alpha}^{x_{J+1/2}} A(\hat{x}_l^\alpha, v) n_h(t, v) dv + \sum_{i=J+1}^{N} \int_{I_i} A(\hat{x}_l^\alpha, v) n_h(t, v) dv.$$

By the Gaussian quadrature formula (2.3), the integral terms can be approximated as

$$\Gamma_{j,l}^\alpha = \frac{1}{2}(b_J - a_J) \sum_{\beta=1}^{Q} \omega_\beta A(\hat{x}_l^\alpha, y_J^\beta) n_h(t, y_J^\beta) + \sum_{i=J+1}^{N} \frac{h_i}{2} \sum_{\beta=1}^{Q} \omega_\beta A(\hat{x}_l^\alpha, \hat{x}_i^\beta) n_h(t, \hat{x}_i^\beta), \tag{2.5}$$

where $a_J = x_{j+1/2} - \hat{x}_l^\alpha$, $b_J = x_{J+1/2}$, and the quadrature points in the first term are given by

$$y_J^\beta = \frac{1}{2}(b_J + a_J) + \frac{1}{2}(b_J - a_J) s_\beta.$$

To be more precise, the index J depends on j, l, and α. Note that in (2.5) the polynomial function n_h has to be evaluated at intermediate points y_J^β for the approximation of the integral part here.

Next, we evaluate the breakage flux

$$F_b(t, x_{j+1/2}) = -\int_{x_{j+1/2}}^{x_{N+1/2}} \int_0^{x_{j+1/2}} B(u, v) n_h(t, v) du dv = -\sum_{l=j+1}^{N} \int_{I_l} n_h(t, v) G_j(v) dv$$

with the partial flux

$$G_j(v) = \sum_{i=1}^{j} \int_{I_i} B(u, v) du$$

by the numerical flux

$$F_{b,j+1/2} = -\sum_{l=j+1}^{N} \frac{h_l}{2} \sum_{\alpha=1}^{Q} \omega_\alpha n_h(t, \hat{x}_l^\alpha) G_{j,l}^\alpha, \tag{2.6}$$

where $G_{j,l}^\alpha$ is an approximation to the partial flux $G_j(\hat{x}_l^\alpha)$ and is given by

$$G_{j,l}^\alpha = \sum_{i=1}^{j} \frac{h_i}{2} \sum_{\beta=1}^{Q} \omega_\beta B(\hat{x}_i^\beta, \hat{x}_l^\alpha). \tag{2.7}$$

Now, let us consider the second term in the DG scheme (2.2). We apply again Gaussian quadrature of order Q for the approximation of the integral,

$$\int_{I_j} F_h \partial_x \phi \, dx = \int_{-1}^{1} F_h \partial_\xi \phi \, d\xi \approx \sum_{\gamma=1}^{Q} \omega_\gamma \phi'(s_\gamma) F_h(t, \hat{x}_j^\gamma). \tag{2.8}$$

The approximation of the flux at the Gauss points, $F_h(t, \hat{x}_j^\gamma)$, is very similar to the approximation of the boundary terms above and is shown in Appendix A.

Remark 2.1. For the approximation of the integral over a cell I_j, we consider the Q-point Gaussian quadrature which is accurate for polynomials up to degree $2Q-1$. In case of a linear and local flux function, F would be of polynomial degree k and ϕ' would have maximal degree $k-1$, in total $2k-1$, corresponding to $Q=k$ Gauss points. In our case, the flux is nonlocal, and quadrature rules are also needed for the evaluation of the flux. Note that $Q=k$ would be enough to make the scheme consistent. However, for our simulations we have chosen $Q=k+1$ since we observe an interesting type of superconvergence in this case which we will demonstrate in the numerical tests; see section 4. For simplicity, we choose the same Q for the numerical approximation of the partial fluxes which is not necessary.

2.3. Time discretization and positivity. By taking the forward Euler discretization in time to (2.2), we obtain a fully discrete scheme

$$\int_{I_j} \frac{n_h^{m+1}-n_h^m}{\Delta t}\phi\,dx - \int_{I_j} F_h^m\phi_x\,dx + F_h^m\phi\,\big|_{\partial I_j} = 0. \tag{2.9}$$

Define the cell average of $n_h(x)$ on I_j by

$$\bar{n}_j := \frac{1}{h_j}\int_{I_j} n_h(x)\,dx. \tag{2.10}$$

Let $\phi = \frac{\Delta t}{h_j}$ so that

$$\bar{n}_j^{m+1} = \bar{n}_j^m - \lambda_j[F_{j+1/2}^m - F_{j-1/2}^m], \quad \lambda_j = \Delta t/h_j. \tag{2.11}$$

Due to the exactness of quadrature rule for polynomials of degree $2k+1$, and especially of degree k, we have

$$\bar{n}_j^m = \frac{1}{h_j}\int_{I_j} n_h^m(x)dx = \frac{1}{2}\sum_{\alpha=1}^{Q}\omega_\alpha n_h^m(\hat{x}_j^\alpha). \tag{2.12}$$

For the proof of the following theorem, we take a closer look at the differences of the flux at two neighboring interfaces. The flux difference for F_a at time level m can be reorganized to

$$F_{a,j+1/2}^m - F_{a,j-1/2}^m = -\sum_{l=1}^{j-1}\frac{h_l}{2}\sum_{\alpha=1}^{Q}\omega_\alpha n_h^m(\hat{x}_l^\alpha)\left(\Gamma_{j-1,l}^\alpha - \Gamma_{j,l}^\alpha\right) + \frac{h_j}{2}\sum_{\alpha=1}^{Q}\omega_\alpha n_h^m(\hat{x}_j^\alpha)\Gamma_{j,j}^\alpha,$$

where the two terms on the right-hand side can be seen as a type of birth and death term, respectively. For use in the following theorem, define the first term as

$$B_{a,j} = \sum_{l=1}^{j-1}\frac{h_l}{2}\sum_{\alpha=1}^{Q}\omega_\alpha n_h^m(\hat{x}_l^\alpha)\left(\Gamma_{j-1,l}^\alpha - \Gamma_{j,l}^\alpha\right).$$

Similarly, the flux difference for F_b at time level m can be combined to

$$F_{b,j+1/2}^m - F_{b,j-1/2}^m = -\sum_{l=j+1}^{N}\frac{h_l}{2}\sum_{\alpha=1}^{Q}\omega_\alpha n_h^m(\hat{x}_l^\alpha)\left(G_{j,l}^\alpha - G_{j-1,l}^\alpha\right) + \frac{h_j}{2}\sum_{\alpha=1}^{Q}\omega_\alpha n_h^m(\hat{x}_j^\alpha)G_{j-1,j}^\alpha.$$

Note that $G_{j,l}^\alpha - G_{j-1,l}^\alpha \geq 0$ and $G_{j-1,j}^\alpha \geq 0$.

THEOREM 2.2. *The high order scheme* (2.11) *preserves the positivity, i.e., assuming the numerical solution* n_h^m *at time level* t_m *to be positive at all points* $\hat{x}_j^\alpha$*; then* $\bar{n}_j^{m+1} > 0$ *under the CFL condition*

$$\Delta t < \frac{1}{\max_{j,\alpha}\left((\Gamma_{j,j}^\alpha)_+ + G_{j-1,j}^\alpha + \frac{1}{h_j \bar{n}_j^m}(-B_{a,j})_+\right)}, \tag{2.13}$$

where $(\cdot)_+$ *denotes* $\max\{\cdot, 0\}$.

Proof. We rewrite scheme (2.11), using (2.12), as

$$\begin{aligned}
\bar{n}_j^{m+1} &= \bar{n}_j^m - \lambda_j[F_{j+1/2} - F_{j-1/2}] \\
&= \bar{n}_j^m - \lambda_j \left[\frac{h_j}{2}\sum_{\alpha=1}^{Q}\omega_\alpha n_h^m(\hat{x}_j^\alpha)\Gamma_{j,j}^\alpha - \sum_{l=1}^{j-1}\frac{h_l}{2}\sum_{\alpha=1}^{Q}\omega_\alpha n_h^m(\hat{x}_l^\alpha)\left(\Gamma_{j-1,l}^\alpha - \Gamma_{j,l}^\alpha\right)\right] \\
&\quad - \lambda_j \left[\frac{h_j}{2}\sum_{\alpha=1}^{Q}\omega_\alpha n_h^m(\hat{x}_j^\alpha)G_{j-1,j}^\alpha - \sum_{l=j+1}^{N}\frac{h_l}{2}\sum_{\alpha=1}^{Q}\omega_\alpha n_h^m(\hat{x}_l^\alpha)\left(G_{j,l}^\alpha - G_{j-1,l}^\alpha\right)\right] \\
&\geq \frac{1}{2}\sum_{\alpha=1}^{Q}\omega_\alpha n_h^m(\hat{x}_j^\alpha)\left[1 - \Delta t\,\Gamma_{j,j}^\alpha - \Delta t\,G_{j-1,j}^\alpha - \Delta t\,\frac{1}{h_j\bar{n}_j^m}(-B_{a,j})\right].
\end{aligned}$$

Therefore, $\bar{n}_j^{m+1} > 0$ under the restriction on the time step (2.13). ∎

Remark 2.3. The CFL condition is somewhat inconvenient, but this condition is only sufficient. For aggregation, in most practical cases the term $B_{a,j}$ is positive, and hence the third term of the condition vanishes. For breakage, the condition depends only on the breakage kernel and the maximal grid point leading to a very restrictive time step. Fortunately, in most cases the time step can be chosen much larger without losing positivity.

2.4. A scaling limiter. Theorem 2.2 implies that in order to preserve the solution positivity, we need to enforce $n_h^m(\hat{x}_j^\alpha) \geq 0$. This is achieved by a reconstruction step using cell averages as a reference.

Let $n_h \in P^k(I_j)$ be an approximation of a smooth function $g(x) \geq 0$ with the cell average $\bar{n}_j$, defined in (2.10). Following the idea of a scaling limiter in [41], we define the scaled polynomial by

$$\tilde{n}_h(x) = \theta\,(n_h(x) - \bar{n}_j) + \bar{n}_j, \quad \theta = \min\left\{1, \frac{\bar{n}_j}{\bar{n}_j - \min_{x\in S_j} n_h(x)}\right\}, \tag{2.14}$$

where

$$S_j = \{\hat{x}_j^\alpha, \alpha = 1, \ldots, Q\}.$$

It is easy to check that the cell average of $\tilde{n}_h$ is still $\bar{n}_j$. Following [41, 24], we have the next lemma.

LEMMA 2.4. *If* $\bar{n}_j > 0$*, then the modified polynomial satisfies*

$$\tilde{n}_h(x) \geq 0 \qquad \textit{for all } x \in S_j.$$

Furthermore, it is as accurate as n_h *in the following sense:*

$$|\tilde{n}_h(x) - n_h(x)| \leq C_k \|n_h - g\|_\infty \qquad \textit{for all } x \in I_j, \tag{2.15}$$

where C_k *is a constant depending on the polynomial degree* k.

Remark 2.5. Lemma 2.4 establishes that the reconstructed polynomial is as accurate as the original polynomial. Our numerical results based on this reconstruction are excellent. It would be interesting to analyze how the reconstruction error will accumulate in time.

3. Implementation details. We would like to introduce the matrix formulation of our numerical scheme and outline the flowchart of the algorithm.

3.1. Matrix formulation and implementation. As a basis for the set of test functions we choose the Legendre polynomials, denoted by $\phi_i(\xi)$,

$$\phi_0(\xi) = 1, \quad \phi_1(\xi) = \xi, \quad \phi_2(\xi) = \tfrac{1}{2}\left(3\xi^2 - 1\right), \ldots \quad \phi := (\phi_0, \ldots, \phi_k)^T,$$

which are orthogonal in $L^2([-1,1])$. On each cell, the unknown function can be represented as

$$n_h(t,x) = \sum_{i=0}^{k} n_j^i(t)\phi_i(\xi^j(x)), \quad x \in I_j.$$

Here $\xi^j(x)$ is the mapping from I_j to $[-1,1]$, $\xi^j(x) := \frac{2}{h_j}(x - x_j)$. To determine n_h, it suffices to identify the coefficients $n_j = (n_j^0, \ldots, n_j^k)^T$. Due to the orthogonality of the basis functions, the mass matrix becomes diagonal,

$$\int_{I_j} \partial_t n_h \phi \, dx = \frac{h_j}{2} \int_{-1}^{1} \phi(\xi)\phi^T(\xi) d\xi \, \frac{d}{dt} n_j(t) = \frac{h_j}{2} \, \mathrm{diag}\{c_0, \ldots, c_k\} \, \frac{d}{dt} n_j(t), \tag{3.1}$$

where $c_i = \frac{2}{2i+1}$ are the normalization constants.

The fact that we only require n_h^m to be positive at certain points can reduce the computational cost considerably. Instead of finding the minimum of n_h on the whole computational cell I_j, we take the minimum only on the test set S_j.

3.2. Algorithm flowchart. In (2.9), we give a fully discretized scheme using the Euler forward time stepping. For a higher order time discretization, we consider an algorithm with the strong stability preserving (SSP)-RK method [12]. It can be implemented by repeating the following flowchart in each stage since each SSP-RK method is a convex linear combination of the forward Euler. For our numerical simulations, we use a low storage explicit 5-stage fourth order RK method, given in [13, p. 64]. The desired positivity-preserving property is ensured under a suitable CFL condition:

(1) Initialization: From the given initial data $n_0(x)$,
   (i) generate $n_h^0 \in V_h^k$ by piecewise L^2 projection, and
   (ii) reconstruct n_h^0 as in step (3).
(2) Evolution: Use the scheme (2.9) to compute n_h^{m+1}.
   (i) If $\bar{n}_j^{m+1}$ is positive for all j, set $n_h^m = n_h^{m+1}$, and continue with step (3).
   (ii) Otherwise, halve the time step Δt and restart step (2).
(3) Reconstruction: Use (2.14) and set $n_h^m = \tilde{n}_h^m$, and continue with step (2).

4. Numerical results. In this section, we give numerical tests for the proposed positivity-preserving DG scheme applied to pure aggregation and breakage and also for the combined processes considering several test problems. The following test cases are chosen similar to those in [18]. We compare our results with some standard numerical methods, the cell average technique (CAT) by Kumar [15] and the finite volume scheme (FVS) by Filbet and Laurençot [11], which is a special case of the

presented DG scheme for $k = 0$. The error calculation for the CAT is based on the number density, $f(t,x)$, whereas all other errors are calculated with respect to the mass density, $n(t,x) = xf(t,x)$.

For this type of equations it is convenient to use a geometric grid,

$$x_{j+1/2} = rx_{j-1/2}.$$

We choose the factor $r = 2^{(30/N)}$ to span about nine orders of magnitude. We set $x_{1/2} = 0$ and $x_{3/2} = x_0$, where x_0 can be adapted to the different cases. Recall that $h = \max_j h_j$. The time step Δt is chosen to be very small in order to reduce numerical errors due to the time discretization.

All numerical simulations below were carried out to investigate the experimental order of convergence (EOC). The error is measured in a continuous and a discrete norm. The continuous L^1 norm can be approximated by

$$e_h = \sum_j \frac{h_j}{2} \sum_{\alpha=1}^{R} \tilde{\omega}_\alpha |n_h(t, \tilde{x}_j^\alpha) - n(t, \tilde{x}_j^\alpha)|, \tag{4.1}$$

using a high order Gaussian quadrature rule, where $\tilde{\omega}_\alpha > 0$ are the weights and $\tilde{x}_j^\alpha$ are the corresponding Gauss points in each cell I_j. We choose $R = 16$ through all the examples. The symbol h corresponds to the number of cells. The discrete L^1 norm is given by

$$e_{h,d} = \sum_j \frac{h_j}{2} \sum_{\alpha=1}^{Q} \omega_\alpha |n_h(t, \hat{x}_j^\alpha) - n(t, \hat{x}_j^\alpha)|, \tag{4.2}$$

where the Gaussian quadrature points are the same as used for the discretization of the scheme. We have chosen the L^1 norm since it is a natural choice for conservation laws. Using the L^2 or L^∞ norm, similar numerical results and the same order of convergence can be obtained. The error calculation in the discrete norm coincides for $k = 0$ with that used by Filbet and Laurençot [11] for the FVS.

If the problem has analytical solutions, the following formula is used to calculate the EOC:

$$\mathrm{EOC} = \ln(e_h/e_{h/2})/\ln(2),$$

where e_h corresponds to N number of cells and $e_{h/2}$ corresponds to $2N$ cells. In case of the unavailability of the analytical solutions, the EOC can be computed using $e_h = \|n_h - n_{h/2}\|$, where $n_{h/2}$ is interpolated onto the grid of n_h by a high order polynomial interpolation. For the calculation of the EOC, we show the numerical errors at time $t = 0.01$ since the order of convergence of the DG scheme after longer times is disturbed by the low order time integration.

We shall also evaluate the moments of the numerical solution by

$$M_{p,h} = \int_0^L x^{p-1} n_h(t,x)dx = \sum_j \frac{h_j}{2} \sum_{\alpha=1}^{R} \tilde{\omega}_\alpha (\tilde{x}_j^\alpha)^{p-1} n_h(t, \tilde{x}_j^\alpha), \quad p = 0, 1, 2, \ldots,$$

where R is chosen large enough such that the integration is exact for all moments under consideration. The error in the moments is then given by

$$e(M_{p,h}) = \frac{|M_{p,h} - M_p|}{M_p}, \quad p = 0, 1, 2, \ldots,$$

where the error in the first moment $e(M_{1,h})$ of course vanishes by the construction of the method.

4.1. Pure aggregation.

Test case 1. The numerical verification of the EOC of the DG solutions for aggregation is discussed by taking three problems, namely the case of constant, sum, and product aggregation kernels. The analytical solutions for these problems taking the exponential initial distribution $n(0,x) = x\exp(-x)$ have been given by Scott [37]. The computational domain in these cases is taken as $[10^{-3}, 10^6]$.

The numerical solutions for the sum aggregation kernel with $N = 15$ cells and different polynomial degree k are shown in Figure 4.1. The numerical solution is shown together with the analytical one at time $t = 3$, where the degree of aggregation is $I_{\text{agg}} = 1 - M_0(t)/M_0(0) \approx 95\%$. Due to the logarithmic scale of the x-axis, the piecewise linear solution for $k = 1$ appears curved and also the Gauss points are of course symmetrically distributed in one cell. Obviously, the approximation improves for a higher polynomial degree.

The numerical errors for the sum aggregation kernel are shown in Tables 4.1 and 4.2. In the continuous L^1 norm, the EOC is $k + 1$, as expected. In the discrete

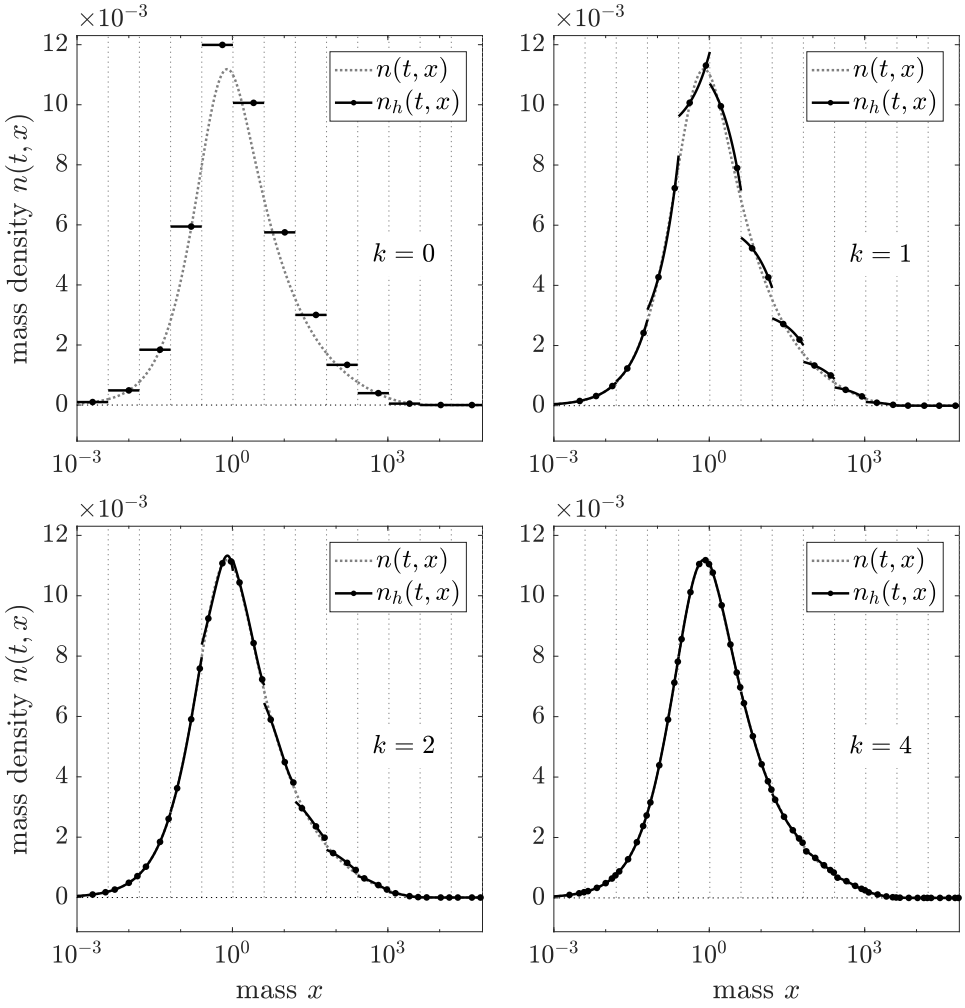

FIG. 4.1. *Numerical solution for $N = 15$ cells and different k for test case* 1.

TABLE 4.1
L^1 errors e_h and EOC for test case 1.

$k\backslash N$	15	30	60	120	240	EOC
0 (FVS)	4.2e-1	2.1e-1	1.0e-1	5.2e-2	2.6e-2	1.0
1	1.3e-1	4.4e-2	1.1e-2	2.8e-3	6.9e-4	2.0
2	7.4e-2	8.0e-3	1.1e-3	1.4e-4	1.7e-5	3.0
4	1.3e-2	3.0e-4	1.0e-5	3.3e-7	1.0e-8	5.0
8	3.6e-5	3.7e-7	7.0e-10	1.4e-12	1.2e-14	9.0
CAT	5.3e-1	2.3e-1	1.1e-1	5.3e-2	2.6e-2	1.0

TABLE 4.2
Discrete L^1 errors $e_{h,d}$ and EOC for test case 1.

$k\backslash N$	15	30	60	120	240	EOC
0 (FVS)	1.3e-1	5.5e-2	1.4e-2	3.5e-3	8.8e-4	2.0
1	8.7e-2	9.0e-3	1.2e-3	1.5e-4	1.8e-5	3.0
2	3.8e-2	1.9e-3	1.1e-4	6.8e-6	4.3e-7	4.0
4	3.6e-3	5.2e-5	9.4e-7	1.5e-8	2.3e-10	6.0
8	2.9e-5	4.7e-8	6.0e-11	6.6e-14	2.0e-14	10.0
CAT	1.3e-1	3.7e-2	9.6e-3	2.4e-3	6.1e-4	2.0

L^1 norm, the EOC is $k+2$ on a geometric grid which is one order higher than in the continuous norm. It appears that the evaluation of the numerical solution at the same Gauss points as used for the discretization of the scheme shows a type of superconvergence. For $k=0$, the second order convergence for the FVS on smooth grids was proven in [18].

The numerical results for the constant and product aggregation kernels are very similar and are not shown again. In our tests, we observe that even the postgelation phase [9] for the product aggregation kernel can be simulated very well.

The evolution of the numerical error in time is shown for the constant aggregation kernel in Figure 4.2(left). We show the results for $N=30$ cells and varying polynomial degree k up to time $t=1000$, where the degree of aggregation is $I_{\text{agg}} \approx 99.8\%$. One can observe that the numerical error remains bounded for longer times.

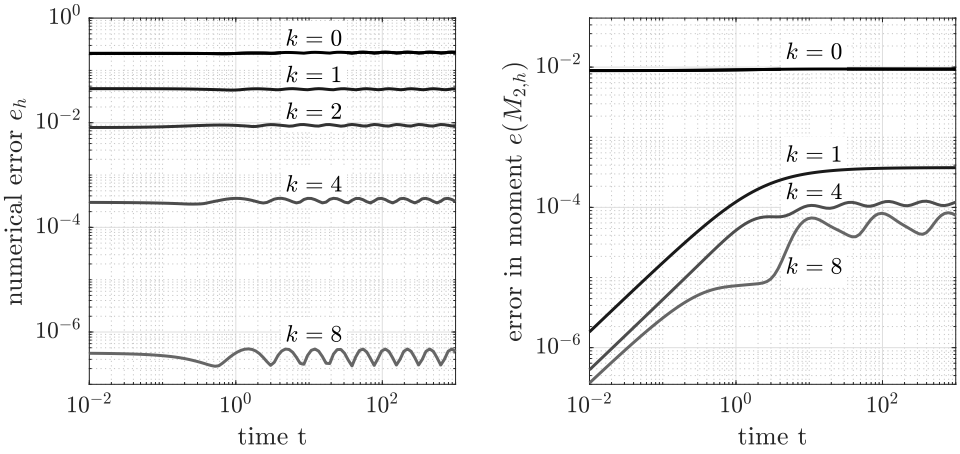

FIG. 4.2. *Error evolution of n_h for $N=30$ and different k (left) and of the second moment for $N(k+1)=90$ (right) for test case 1.*

TABLE 4.3
Numerical errors in the first six moments for test case 1.

(N,k)	$e(M_{0,h})$	$e(M_{1,h})$	$e(M_{2,h})$	$e(M_{3,h})$	$e(M_{4,h})$	$e(M_{5,h})$
FVS (90, 0)	6.6e-3	0	9.4e-3	3.7e-2	8.6e-2	1.6e-1
(45, 1)	2.8e-4	0	3.7e-4	3.8e-3	1.6e-2	4.5e-2
(30, 2)	6.7e-5	0	6.2e-4	2.2e-3	3.6e-3	1.5e-3
(18, 4)	9.1e-6	0	1.2e-4	6.1e-4	3.1e-3	1.6e-2
(10, 8)	5.1e-6	0	7.7e-5	7.6e-4	8.2e-3	4.6e-2
CAT (90)	3.7e-14	0	1.1e-2	2.9e-2	5.1e-2	7.3e-2

In this test case, we also discuss the approximation of the moments. The errors in the first six moments $M_0, \ldots, M_5$ for the constant aggregation kernel at time $t = 1000$ are shown in Table 4.3. For a better comparison, we have chosen the same number of evaluation points $N(k+1) = 90$. One can see that the prediction of the zeroth moment is very accurate and even the higher moments are approximated well. The lower moments are predicted better for an increasing polynomial degree k. The accuracy in the higher moments for a larger polynomial degree k is disturbed by some small oscillations of the piecewise high order polynomial for large values of x. For the CAT, we have to use the normalized moments $\tilde{M}_{p,h}(t) = M_{p,h}(t)/M_{p,h}(0)$ for the error calculation of the moments, $e(\tilde{M}_{p,h})$, since the discretization is focused on the number density and even the first moment has a discretization error in the initial distribution. The first two moments are preserved exactly by the construction of the method, and it produces errors similar to those of the FVS for the higher moments.

In Figure 4.2(right), we have shown the evolution of the error in the second moment $e(M_{2,h})$ in time for different k again with the same number of evaluation points $N(k+1) = 90$. One can observe that the error in the moments increases initially but remains bounded for longer times.

4.2. Pure breakage.

Test case 2. Here, the EOC is calculated for the binary breakage $b(x, y) = 2/y$ together with the linear and quadratic selection functions, i.e., $S(x) = x$ and $S(x) = x^2$. The analytical solutions for such problems have been given by Ziff and McGrady [43] for an exponential initial condition, $n(0, x) = x\exp(-x)$. The computational domain in these cases is taken as $[10^{-6}, 10^3]$.

TABLE 4.4
L^1 errors e_h and EOC for test case 2.

$k\backslash N$	15	30	60	120	240	EOC
0 (FVS)	4.2e-1	2.1e-1	1.0e-1	5.2e-2	2.6e-2	1.0
1	1.3e-1	4.5e-2	1.1e-2	2.8e-3	6.9e-4	2.0
2	7.0e-2	8.0e-3	1.1e-3	1.4e-4	1.7e-5	3.0
4	1.3e-2	3.1e-4	1.0e-5	3.3e-7	1.0e-8	5.0
8	2.5e-5	4.2e-7	7.4e-10	1.4e-12	1.2e-14	9.0
CAT	5.3e-1	2.3e-1	1.1e-1	5.3e-2	2.6e-2	1.0

The results for the linear selection function are shown in Table 4.4. Hence, we observe that the DG scheme is $k+1$ order convergent in the L^1 norm. Similar to the previous case, the order of convergence is $k+2$ using the discrete L^1 norm, which is not shown again. For $k = 0$, the second order convergence was proven in [18] to be mesh-independent for breakage. The results for the quadratic selection function are very similar and are omitted. Also, the behavior of the error evolution and the error in the moments is similar and is not shown again.

In this example, we want to show that the reconstruction step using a scaling limiter is necessary for the stability of the numerical scheme. Consider a linear selection function $S(x) = x$, and choose $N = 6$ cells and $k = 3$, i.e., cubic polynomials. The CFL condition is then given by

$$\Delta t < \frac{1}{\max_{j,\alpha}\left(G^{\alpha}_{j-1,j}\right)} = \frac{1}{G^{1}_{N-1,N}} = \frac{\hat{x}^{1}_{N}}{(x_{N-1/2})^2} \approx 0.0939.$$

Now, using the SSP-RK4 method with a constant time step of $\Delta t = 0.01$ we observe that the numerical solution produces oscillations at the tail of the size distribution and blows up in finite time; see Figure 4.3. Only for $\Delta t \leq 0.005$ do we observe a stable solution without using a reconstruction step. This is a significant restriction. With the use of the scaling limiter presented above, we observe that no negative values are generated by the scheme and therefore the solution remains stable, even when raising the time step to $\Delta t = 1$. This shows that the scaling limiter is necessary for a reasonable time discretization of the DG scheme.

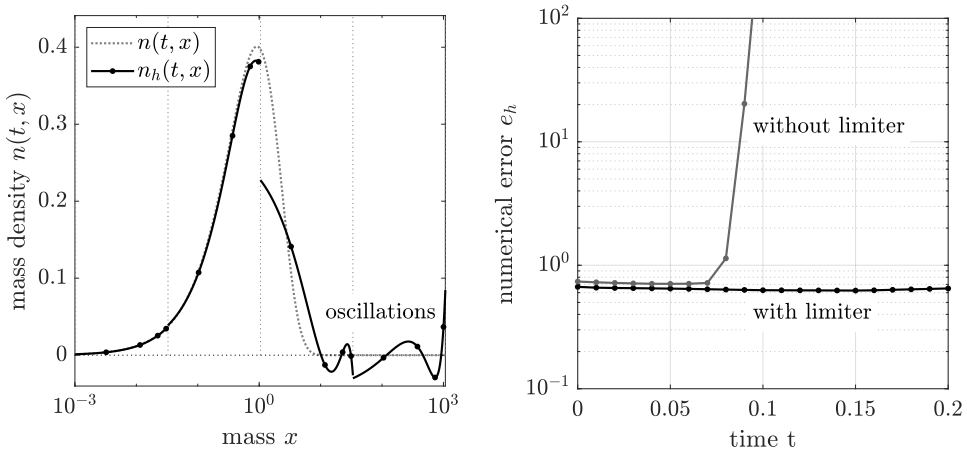

FIG. 4.3. *Numerical solution for $N = 6$ and $k = 3$ without a scaling limiter at time $t = 0.09$ (left) and evolution of the numerical error with and without a scaling limiter (right).*

Test case 3. Now, the case of multiple breakage with the quadratic selection function $S(x) = x^2$ is considered where an analytical solution is not known. For the numerical simulations, the following normal distribution as an initial condition is taken:

$$n(0,x) = \frac{x}{\sigma\sqrt{2\pi}} \exp\left(-\frac{(x-\mu)^2}{2\sigma^2}\right).$$

The computations are made for the breakage function considered by Hill and Ng [14]:

$$b(x,y) = p\left(\frac{[m+(m+1)(p-1)]!}{m![m+(m+1)(p-2)]!}\right)\frac{x^m(y-x)^{m+(m+1)(p-2)}}{y^{pm+p-1}}, \quad p \in \mathbb{N},\ p \geq 2,$$

where the relation $\int_0^y b(x,y)dx = p$ holds, where p gives the total number of fragments per breakage event. The parameter $m \geq 0$ is responsible for the shape of the daughter particle distribution. The numerical solutions are obtained using $p = 4$, $m = 2$.

For the numerical simulation, the computational domain is taken as $[10^{-6}, 10^{3}]$. In this case, the numerical error e_h is computed from the numerical solutions n_h and

$n_{h/2}$, as mentioned above. As expected, we again observe from Table 4.5 that the DG scheme shows convergence of order $k+1$. Using the discrete L^1 norm, we again obtain the higher convergence order $k+2$.

TABLE 4.5
L^1 errors e_h and EOC for test case 3.

$k\backslash N$	15	30	60	120	240	EOC
0 (FVS)	5.5e-1	2.5e-1	1.1e-1	6.6e-2	3.3e-2	1.0
1	1.7e-1	5.5e-2	1.4e-2	3.5e-3	8.8e-4	2.0
2	3.0e-2	1.3e-2	1.6e-3	2.0e-4	2.6e-5	3.0
4	1.4e-2	5.8e-4	1.6e-5	5.6e-7	1.7e-8	5.0
8	4.0e-4	1.5e-7	1.6e-9	3.1e-12	8.2e-14	9.0
CAT	3.0e-1	1.1e-1	4.6e-2	2.1e-2	1.0e-2	1.0

4.3. Coupled aggregation-breakage.

Test case 4. Finally, the EOC is evaluated for the simultaneous process with a constant aggregation kernel $K(x,y)=1$ and breakage kinetics $b(x,y)=2/y$, $S(x)=x/2$. For the simulation, the computational domain $[10^{-3},10^{6}]$ is taken. The analytical solutions for this problem are given by Lage [20] for the following two different initial conditions:

$$n(0,x) = x\mathrm{e}^{-x},$$
$$n(0,x) = 4x^2\mathrm{e}^{-2x}.$$

The former exponential initial condition is a steady state solution. The latter Gaussian-like initial condition is a special case where the number of particles stays constant. From Table 4.6, we find that the DG scheme is $k+1$ order convergent where the results for the first case are shown. As before, we obtain one order higher convergence on a geometric grid in the discrete norm. The second case is very similar and is omitted.

TABLE 4.6
L^1 errors e_h and EOC for test case 4.

$k\backslash N$	15	30	60	120	240	EOC
0 (FVS)	4.2e-1	2.1e-1	1.1e-1	5.2e-2	2.6e-2	1.0
1	1.3e-1	4.5e-2	**1.1e-2**	2.8e-3	6.9e-4	2.0
2	7.4e-2	8.1e-3	1.1e-3	1.4e-4	1.7e-5	3.0
4	**1.3e-2**	3.0e-4	1.0e-5	3.3e-7	1.0e-8	5.0
8	3.9e-5	4.0e-7	7.3e-10	1.4e-12	4.2e-15	9.0
CAT	5.3e-1	2.3e-1	1.1e-1	5.3e-2	2.6e-2	1.0

All test cases demonstrate the advantage of the high order DG method over the lower order methods. For a high accuracy, only the use of high values of k is suitable, and even for a moderate accuracy, the high order method may be better suited. Consider, for example, an error tolerance of about 1.3×10^{-2}. In Table 4.6, we observe that for $k=0$ one needs $N=480$ cells due to the linear convergence. With the same error tolerance, the number of cells needed is decreased considerably to $N=60,15$ for $k=1,4$, respectively. This shows clearly the significance of the proposed DG scheme.

5. Concluding remarks. In this paper, we have developed a high order DG scheme which can be proven to be positivity-preserving for both coagulation and

fragmentation equations. We have tested the DG scheme and clearly observed the convergence order $k+1$ and the strict positivity preservation in all these tests. Interestingly, the DG scheme shows a type of superconvergence of order $k+2$ on a geometric grid in the discrete norm which evaluates the numerical solution at the same Gaussian quadrature points as used for the discretization of the scheme. Even though the CFL condition derived to preserve positivity might be very restrictive in some cases, we emphasize that it is not a necessary condition and can be relaxed significantly. The high accuracy was verified numerically by taking various examples of pure aggregation, pure breakage, and the combined problems.

By applying the limiter or the simplified version, which avoids the evaluation of extrema of polynomials, to a discontinuous Galerkin scheme solving one-dimensional coagulation-fragmentation equations, with the time evolution by an SSP-RK method, we obtain a high order accurate scheme with strict positivity preservation.

Appendix A. In subsection 2.2, we have shown the flux evaluation for the boundary term in the DG scheme (2.2). For the numerical approximation of the second term, we apply Gaussian quadrature, as already shown in (2.8). The approximation of the flux at the Gauss points, $F_h(t,\hat{x}_j^\gamma)$, is shown in the following.

For aggregation, the flux $F_a(t,\hat{x}_j^\gamma)$ can be approximated by the numerical flux

$$F_{a,j}^\gamma = \sum_{l=1}^{j} \frac{b_l - a_l}{2} \sum_{\alpha=1}^{Q} \omega_\alpha n_h(t,u_l^\alpha)\Gamma_{j,l}^{\gamma,\alpha}, \tag{A.1}$$

where $a_l = x_{l-1/2}$, $b_l = x_{l+1/2}$ for $l<j$ and $b_l = \hat{x}_j^\gamma$ for $l=j$, and $u_l^\alpha = \frac{1}{2}(b_l+a_l) + \frac{1}{2}(b_l-a_l)s_\alpha$. The partial flux $\Gamma_j^\gamma(u_l^\alpha)$ is approximated by

$$\Gamma_{j,l}^{\gamma,\alpha} = \frac{1}{2}(b_J - a_J)\sum_{\beta=1}^{Q}\omega_\beta A(u_l^\alpha, y_J^\beta)n_h(t,y_J^\beta) + \sum_{i=J+1}^{N}\frac{h_i}{2}\sum_{\beta=1}^{Q}\omega_\beta A(u_l^\alpha,\hat{x}_i^\beta)n_h(t,\hat{x}_i^\beta), \tag{A.2}$$

where $a_J = \hat{x}_j^\gamma - u_l^\alpha$, $b_J = x_{J+1/2}$, and $y_J^\beta = \frac{1}{2}(b_J+a_J) + \frac{1}{2}(b_J-a_J)s_\beta$. The index J is chosen such that $\hat{x}_j^\gamma - u_l^\alpha \in I_J$. Here, the index J depends on j, γ, l, and α.

For breakage, the flux $F_b(t,\hat{x}_j^\gamma)$ is approximated by

$$F_{b,j}^\gamma = -\sum_{l=j}^{N}\frac{b_l-a_l}{2}\sum_{\alpha=1}^{Q}\omega_\alpha n_h(t,u_l^\alpha)G_{j,l}^{\gamma,\alpha}, \tag{A.3}$$

where $a_l = \hat{x}_j^\gamma$ for $l=j$ and $a_l = x_{l-1/2}$ for $l>j$, $b_l = x_{l+1/2}$, and $u_l^\alpha = \frac{1}{2}(b_l+a_l) + \frac{1}{2}(b_l-a_l)s_\alpha$. The partial flux $G_j^\gamma(u_l^\alpha)$ is approximated by

$$G_{j,l}^{\gamma,\alpha} = \sum_{i=1}^{j}\frac{b_i-a_i}{2}\sum_{\beta=1}^{Q}\omega_\beta B(u_i^\beta, u_l^\alpha), \tag{A.4}$$

where $a_i = x_{i-1/2}$, $b_i = x_{i+1/2}$ for $i<j$ and $b_i = \hat{x}_j^\gamma$ for $i=j$, and $u_i^\beta = \frac{1}{2}(b_i+a_i) + \frac{1}{2}(b_i-a_i)s_\beta$.

REFERENCES

[1] D. J. Aldous, *Deterministic and stochastic models for coalescence (aggregation and coagulation): A review of the mean-field theory for probabilists*, Bernoulli, 5 (1999), pp. 3–48, https://doi.org/10.2307/3318611.

[2] J. P. Bourgade and F. Filbet, *Convergence of a finite volume scheme for coagulation-fragmentation equations*, Math. Comp., 77 (2008), pp. 851–882, https://doi.org/10.1090/S0025-5718-07-02054-6.

[3] G. Chavent and B. Cockburn, *The local projection P^0-P^1-discontinuous-Galerkin finite element method for scalar conservation laws*, RAIRO Modél. Math. Anal. Numér., 23 (1989), pp. 565–592, https://doi.org/10.1051/m2an/1989230405651.

[4] B. Cockburn and C.-W. Shu, *TVB Runge-Kutta local projection discontinuous Galerkin finite element method for conservation laws* II: *General framework*, Math. Comp., 52 (1989), pp. 411–435, https://doi.org/10.1090/S0025-5718-1989-0983311-4.

[5] B. Cockburn and C.-W. Shu, *The Runge-Kutta local projection P^1-discontinuous-Galerkin finite element method for scalar conservation laws*, RAIRO Modél. Math. Anal. Numér., 25 (1991), pp. 337–361, https://doi.org/10.1051/m2an/1991250303371.

[6] B. Cockburn and C.-W. Shu, *Runge-Kutta discontinuous Galerkin methods for convection-dominated problems*, J. Sci. Comput., 16 (2001), pp. 173–261, https://doi.org/10.1023/A:1012873910884.

[7] P. B. Dubovskii, V. A. Galkin, and I. W. Stewart, *Exact solutions for the coagulation-fragmentation equation*, J. Phys. A, 25 (1992), pp. 4737–4744, https://doi.org/10.1088/0305-4470/25/18/009.

[8] L. D. Erasmus, D. Eyre, and R. C. Everson, *Numerical treatment of the population balance equation using a Spline-Galerkin method*, Comput. Chem. Eng., 18 (1994), pp. 775–783, https://doi.org/10.1016/0098-1354(94)E0007-A.

[9] M. H. Ernst, R. M. Ziff, and E. M. Hendriks, *Coagulation processes with a phase transition*, J. Colloid Interface Sci., 97 (1984), pp. 266–277, https://doi.org/10.1016/0021-9797(84)90292-3.

[10] M. Escobedo, P. Laurençot, S. Mischler, and B. Perthame, *Gelation and mass conservation in coagulation-fragmentation models*, J. Differential Equations, 195 (2003), pp. 143–174, https://doi.org/10.1016/S0022-0396(03)00134-7.

[11] F. Filbet and P. Laurençot, *Numerical simulation of the Smoluchowski coagulation equation*, SIAM J. Sci. Comput., 25 (2004), pp. 2004–2028, https://doi.org/10.1137/S1064827503429132.

[12] S. Gottlieb, C.-W. Shu, and E. Tadmor, *Strong stability-preserving high-order time discretization methods*, SIAM Rev., 43 (2001), pp. 89–112, https://doi.org/10.1137/S003614450036757X.

[13] J. S. Hesthaven and T. Warburton, *Nodal Discontinuous Galerkin Methods: Algorithms, Analysis, and Applications*, Texts Appl. Math. 54, Springer, New York, 2008, https://doi.org/10.1007/978-0-387-72067-8.

[14] P. J. Hill and K. M. Ng, *Statistics of multiple particle breakage*, AIChE J., 42 (1996), pp. 1600–1611, https://doi.org/10.1002/aic.690420611.

[15] J. Kumar, *Numerical Approximations of Population Balance Equations in Particulate Systems*, Ph.D. thesis, Otto von Guericke University, Magdeburg, Germany, 2006, http://nbn-resolving.de/urn:nbn:de:101:1-201010182122.

[16] J. Kumar, G. Warnecke, M. Peglow, and S. Heinrich, *Comparison of numerical methods for solving population balance equations incorporating aggregation and breakage*, Powder Technol., 189 (2009), pp. 218–229, https://doi.org/10.1016/j.powtec.2008.04.014.

[17] R. Kumar, J. Kumar, and G. Warnecke, *Moment preserving finite volume schemes for solving population balance equations incorporating aggregation, breakage, growth and source terms*, Math. Models Methods Appl. Sci., 23 (2013), pp. 1235–1273, https://doi.org/10.1142/S0218202513500085.

[18] R. Kumar, J. Kumar, and G. Warnecke, *Convergence analysis of a finite volume scheme for solving non-linear aggregation-breakage population balance equations*, Kinet. Relat. Models, 7 (2014), pp. 713–737, https://doi.org/10.3934/krm.2014.7.713.

[19] S. Kumar and D. Ramkrishna, *On the solution of population balance equations by discretization—*I. *A fixed pivot technique*, Chem. Eng. Sci., 51 (1996), pp. 1311–1332, https://doi.org/10.1016/0009-2509(96)88489-2.

[20] P. L. C. Lage, *Comments on the "An analytical solution to the population balance equation with coalescence and breakage—the special case with constant number of particles" by D.P. Patil and J.R.G. Andrews*, Chem. Eng. Sci., 57 (2002), pp. 4253–4254, https://doi.org/10.1016/S0009-2509(02)00369-X.

[21] W. Lamb, *Existence and uniqueness results for the continuous coagulation and fragmentation equation*, Math. Methods Appl. Sci., 27 (2004), pp. 703–721, https://doi.org/10.1002/mma.496.

[22] K. Lee and T. Matsoukas, *Simultaneous coagulation and break-up using constant-N Monte*

Carlo, Powder Technol., 110 (2000), pp. 82–89, https://doi.org/10.1016/S0032-5910(99)00270-3.

[23] J. Litster and B. Ennis, *The Science and Engineering of Granulation Processes*, Part. Technol. Ser. 15, Springer, Dordrecht, 2004, https://doi.org/10.1007/978-94-017-0546-2.

[24] H. Liu and H. Yu, *Maximum-principle-satisfying third order discontinuous Galerkin schemes for Fokker–Planck equations*, SIAM J. Sci. Comput., 36 (2014), pp. A2296–A2325, https://doi.org/10.1137/130935161.

[25] G. Madras and B. J. McCoy, *Reversible crystal growth-dissolution and aggregation-breakage: Numerical and moment solutions for population balance equations*, Powder Technol., 143-144 (2004), pp. 297–307, https://doi.org/10.1016/j.powtec.2004.04.022.

[26] A. W. Mahoney and D. Ramkrishna, *Efficient solution of population balance equations with discontinuities by finite elements*, Chem. Eng. Sci., 57 (2002), pp. 1107–1119, https://doi.org/10.1016/S0009-2509(01)00427-4.

[27] D. L. Marchisio and R. O. Fox, *Solution of population balance equations using the direct quadrature method of moments*, J. Aerosol Sci., 36 (2005), pp. 43–73, https://doi.org/10.1016/j.jaerosci.2004.07.009.

[28] D. J. McLaughlin, W. Lamb, and A. C. McBride, *Existence and uniqueness results for the non-autonomous coagulation and multiple-fragmentation equation*, Math. Methods Appl. Sci., 21 (1998), pp. 1067–1084, https://doi.org/10.1002/(SICI)1099-1476(19980725)21:11<1067::AID-MMA985>3.0.CO;2-X.

[29] Z. A. Melzak, *A scalar transport equation*, Trans. Amer. Math. Soc., 85 (1957), pp. 547–560, https://doi.org/10.2307/1992943.

[30] S. Motz, A. Mitrović, and E.-D. Gilles, *Comparison of numerical methods for the simulation of dispersed phase systems*, Chem. Eng. Sci., 57 (2002), pp. 4329–4344, https://doi.org/10.1016/S0009-2509(02)00349-4.

[31] H. Müller, *Zur allgemeinen Theorie der raschen Koagulation*, Kolloidchem. Beihefte, 27 (1928), pp. 223–250, https://doi.org/10.1007/BF02558510.

[32] M. Peglow, J. Kumar, G. Warnecke, S. Heinrich, and L. Mörl, *A new technique to determine rate constants for growth and agglomeration with size- and time-dependent nuclei formation*, Chem. Eng. Sci., 61 (2006), pp. 282–292, https://doi.org/10.1016/j.ces.2004.11.071.

[33] S. Qamar and G. Warnecke, *Solving population balance equations for two-component aggregation by a finite volume scheme*, Chem. Eng. Sci., 62 (2007), pp. 679–693, https://doi.org/10.1016/j.ces.2006.10.001.

[34] D. Ramkrishna, *Population Balances: Theory and Applications to Particulate Systems in Engineering*, Academic Press, New York, 2000, http://www.sciencedirect.com/science/book/9780125769709.

[35] B. Rivière, *Discontinuous Galerkin Methods for Solving Elliptic and Parabolic Equations*, SIAM, Philadelphia, 2008, https://doi.org/10.1137/1.9780898717440.

[36] A. Sandu, *Piecewise polynomial solutions of aerosol dynamic equation*, Aerosol Sci. Technol., 40 (2006), pp. 261–273, https://doi.org/10.1080/02786820500543274.

[37] W. T. Scott, *Analytic studies of cloud droplet coalescence* I, J. Atmospheric Sci., 25 (1968), pp. 54–65, https://doi.org/10.1175/1520-0469(1968)025<0054:ASOCDC>2.0.CO;2.

[38] C.-W. Shu, *Discontinuous Galerkin methods: General approach and stability*, in Numerical Solutions of Partial Differential Equations, Birkhäuser, Basel, 2009, pp. 149–201, https://doi.org/10.1007/978-3-7643-8940-6.

[39] M. v. Smoluchowski, *Versuch einer mathematischen Theorie der Koagulationskinetik kolloider Lösungen*, Z. Phys. Chem., 92 (1917), pp. 129–168, https://doi.org/10.1515/zpch-1918-9209.

[40] M. Vanni, *Approximate population balance equations for aggregation-breakage processes*, J. Colloid Interface Sci., 221 (2000), pp. 143–160, https://doi.org/10.1006/jcis.1999.6571.

[41] X. Zhang and C.-W. Shu, *On maximum-principle-satisfying high order schemes for scalar conservation laws*, J. Comput. Phys., 229 (2010), pp. 3091–3120, https://doi.org/10.1016/j.jcp.2009.12.030.

[42] R. M. Ziff, *New solutions to the fragmentation equation*, J. Phys. A, 24 (1991), pp. 2821–2828, https://doi.org/10.1088/0305-4470/24/12/020.

[43] R. M. Ziff and E. D. McGrady, *The kinetics of cluster fragmentation and depolymerisation*, J. Phys. A, 18 (1985), pp. 3027–3037, https://doi.org/10.1088/0305-4470/18/15/026.